JCTC Journal of Chemical Theory and Computation

A Complete Thermodynamic Characterization of Electrostatic and Hydrophobic Associations in the Temperature Range 0 to 100 °C from Explicit-Solvent Molecular Dynamics Simulations

Shun Zhu and Adrian H. Elcock*

Department of Biochemistry, University of Iowa, Iowa City, Iowa 52242

Received February 4, 2010

Abstract: The electrostatic and hydrophobic interactions that dominate the behavior of proteins and other biomolecules exhibit fundamentally different thermodynamic characteristics, and the correct reproduction of these differences is likely to be an important requirement for models that aim to predict the thermodynamics of protein stability and protein−protein interactions. To assess the abilities of some current models to capture these differences, we report here the results of molecular dynamics (MD) simulations examining the association of acetate−methylammonium and methane−methane pairs at 11 different temperatures from −12.5 to 112.5 °C. Simulations were performed using two popular water models (TIP3P and TIP5P), with a total simulation time of 22 μs. With both water models, we find that the acetate−methylammonium salt-bridge interaction is significantly more stabilized by high temperatures (e.g., over the range 25 to 100 °C) than is the methane−methane hydrophobic interaction. At low temperatures however, the two models exhibit quite different behavior, with the TIP5P model predicting little change in the relative stabilities of the two types of interaction in the range −12.5 to 50 °C; this surprising result has potential implications for understanding adaptation to life in psychrophilic organisms. Fitting the ΔG data to the Gibbs−Helmholtz equation allows the ΔH, ΔS, and ΔC_p of interaction to be obtained, thereby yielding a complete thermodynamic characterization of the different types of interaction in the temperature range 0 to 100 °C: despite significant quantitative differences, both water models correctly capture the opposite signs of the ΔC_p of electrostatic and hydrophobic interactions. Finally, we show that at high temperatures a Poisson-based continuum solvation model provides good agreement with the explicit-solvent MD results, but only when the atomic radii used in the continuum calculations are scaled with temperature.

Introduction

In order to fully understand the thermodynamics of protein folding and protein−protein interactions, it is important to know the basic thermodynamic characteristics of the various forces, such as charge−charge and hydrophobic interactions, that drive these processes. A comprehensive thermodynamic characterization of these fundamental types of interactions requires, in turn, not only knowledge of the attendant change in free energy (ΔG) but also the changes in the enthalpy (ΔH), the entropy (ΔS), and the heat capacity (ΔC_p) throughout the temperature range of interest. Since there are "extremophilic" organisms that can survive and thrive at temperatures of 0 °C[1−3] and others that live happily at ∼100 °C,[4−7] a comprehensive understanding of biomolecular thermodynamics in aqueous solution requires us to consider a temperature range of 0° to 100 °C.

Experimental methods such as differential scanning calorimetry and isothermal titration calorimetry have been widely used to study the thermodynamics of protein folding[8−14] and protein−protein interactions,[15−21] respectively, and correlations of the resulting data with structural characteristics of proteins have allowed very useful estimates

* Corresponding author e-mail: adrian-elcock@uiowa.edu.

10.1021/ct1000704
Published on Web 03/01/2010

to be obtained of, for example, the heat capacity change associated with the burial of hydrophobic surface area.[8,22−26] Given, however, that many different types of interactions act simultaneously to determine the thermodynamic properties of proteins, it can be difficult to unambiguously resolve the exact contribution made by a particular type of interaction.[25] One profitable way to circumvent this problem is to apply the same kinds of experimental methods to the study of small molecules that are representative of the components of proteins.[8,27−38] Even here, however, there can be difficulties of interpretation; it is not completely clear, for example, how good a model the commonly used N-methylacetamide is as a model of the polypeptide backbone of proteins.[38]

An alternative but complementary approach to direct experimentation is to use molecular simulation methods to directly measure the thermodynamic features of chosen types of interactions. Although computational results are always subject to concerns about the quality of the underlying force fields,[39,40] the simulation approach has the significant advantage of allowing contributions made by specific types of interactions to be resolved in a highly detailed and structurally unambiguous way: thermodynamic profiles can, for example, be obtained as a function of the distance between the interacting groups in a way that would be difficult, if not impossible, to achieve experimentally. A very large number of molecular simulation studies have already addressed the thermodynamics of hydrophobic associations in this way,[41−56] an abundance of literature that reflects the hydrophobic interaction's apparently dominant role in driving protein folding.[57] The first computed free energy profile for the association of two hydrophobic molecules in explicit solvent was reported many years ago.[58] Subsequent studies[51,55] explored the temperature dependence of the interaction and found, in common with experiment,[59,60] that it became stronger as the temperature increased. Only comparatively recently however have simulation studies been conducted at a sufficient number of different temperatures to allow the ΔC_p of hydrophobic association to be computed precisely.[50,52−54] Continuing this trend, a comprehensive study of the force field dependence of the ΔC_p for hydration and association of hydrophobic atoms has recently been reported,[55] showing that, while the various simulation models lead to quite different magnitudes of the computed ΔC_p, they all correctly reproduce the signs of these ΔC_p's. That a qualitatively correct reproduction of the sign of the ΔC_p for hydrophobic association is a robust prediction of explicit-solvent simulation studies is quite important, since the *negative* ΔC_p is perhaps *the* defining, thermodynamic characteristic feature of protein folding.[61]

In contrast to the wealth of simulation studies that have examined the thermodynamics of the hydrophobic interaction, far less attention has been paid to using explicit-solvent molecular simulations to obtain *complete* thermodynamic characterizations of the other types of interactions that are present in proteins. In particular, very few studies have addressed the thermodynamics of attractive charge−charge interactions beyond measuring the free energy at, for example, 25 °C.[62] Such interactions are, however, likely to be of special interest from a thermodynamic perspective given the apparently critical role of salt bridges (i.e., oppositely charged ion pairs) in the adaptation of proteins to stability at high temperatures.[4−7] Free energy profiles for the association of a Na^+:Cl^- ion pair were first computed using molecular dynamics (MD) simulations many years ago, and a comparison of results obtained at 25° and 100 °C indicated that the higher temperature favored the formation of a contact ion pair.[62] More recently, MD simulations have been used to simulate the diffusive association of lysine and glutamate residues at 25°, 50°, 75°, and 100 °C and to compute free energy profiles for the formation of a prototypical salt bridge at the same temperatures;[63] again, these studies showed the salt bridge interaction to be stabilized by increasing temperature. All of these studies fall far short however of providing the coverage of different temperatures necessary to obtain the ΔC_p associated with the formation of salt bridge interactions. In fact, the only works that we are aware of that have applied molecular simulation methods to explore heat-capacity-related properties of charged groups in aqueous solution are the pioneering studies conducted by the Sharp group aimed at understanding the origins of the ΔC_p of *hydration*.[64−68] These authors used explicit-solvent molecular dynamics (MD) simulations to identify structural features of the hydration shells of hydrophobic and charged atoms that correlate with their opposite signs of the ΔC_p of hydration observed experimentally; since all of their MD simulations were performed at a single temperature, however, they did not explicitly compute the ΔC_p directly from MD simulations.

This work describes the use of MD simulations to obtain a complete thermodynamic characterization of the association of a model salt bridge, the acetate−methylammonium pair, in explicit water and compares its thermodynamic features with those of a model hydrophobic association, the methane−methane interaction, for which we also report new results. Given the demonstration that the magnitudes of ΔC_p estimates can vary significantly depending on the water model used,[55] we have performed complete sets of simulations of both the acetate−methylammonium and methane−methane interactions with two popular water models, TIP3P[69] and TIP5P;[70] these models produced, respectively, the smallest and largest estimates of the ΔC_p of the hydrophobic interaction in the recent wide-ranging study referred to above.[55] The results reported here indicate that both water models reproduce the key qualitative feature that the ΔC_p for the formation of salt bridge and hydrophobic interactions are positive and negative, respectively, although, as expected, they differ significantly in their magnitudes. In addition, the results demonstrate that MD simulations in which associating molecules are allowed to freely diffuse can produce data of sufficient precision to allow ΔC_p to be reliably computed and provide a set of "gold standard" explicit-solvent data against which to compare the predictions of a commonly used implicit-solvent model based on continuum electrostatics.

Methods

Simulation Setup. Molecular dynamics (MD) simulations were conducted at 11 independent temperatures in the range from −12.5 to 112.5 °C: −12.5°, 0°, 12.5°, 25°, 37.5°, 50°,

62.5°, 75°, 87.5°, 100°, and 112.5 °C using the GROMACS v3.3 software.[71,72] All simulations contained either one acetate molecule and one methylammonium molecule or two methane molecules immersed in a 25 × 25 × 25 Å box of water molecules; separate simulations were performed using the TIP3P[69] and TIP5P[70] water models. As in our previous work,[73] the partial charges and van der Waals parameters for the acetate and methylammonium were adapted from those assigned to glutamate and lysine respectively in the OPLS-AA parameter set.[74] A 10 Å cutoff was used for van der Waals and short-range electrostatic interactions, and the Particle Mesh Ewald (PME) method was used to describe all long-range electrostatic interactions.[75] Covalent bonds were constrained with the LINCS algorithm,[76] enabling a 2 fs time step to be used. Simulations were performed in the NPT ensemble, with the pressure being maintained at 1 atm with the Parrinello−Rahman barostat[77] and the temperature being maintained at the desired value with the Nosé-Hoover thermostat.[78,79] Prior to MD, energy minimization was carried out for 100 steps using the steepest-descent algorithm. Each system was then equilibrated for 10 ns before a production simulation lasting 500 ns was conducted, during which atomic coordinates were saved at 0.1 ps intervals, producing 5 million structural snapshots per simulation for analysis. Since all simulations at all temperatures were run for 500 ns, it was possible to obtain converged free energy estimates in almost all cases; the only exceptions were for desolvation barrier regions with the TIP5P water model at <12.5 °C: this water model has a tendency to freeze at low temperatures,[80] which in turn drastically decreases the number of diffusive encounters of the two solutes sampled during each simulation period (Figure S1, Supporting Information).

Free Energy Surface Construction. Two different kinds of free energy surfaces (FESs) were used to describe the association thermodynamics of the molecule pairs. The simplest kind was a one-dimensional FES (also known as a "potential of mean force"; PMF) constructed from histograms of the intermolecular distances extracted from the simulation snapshots.[63] For the acetate−methylammonium pair, this distance was defined in terms of the carboxyl carbon of the acetate molecule and the amino nitrogen of the methylammonium molecule; for the methane−methane pair, the separation distance was defined as the distance between the two carbons. The second kind of FES, used exclusively for the acetate−methylammonium system, was a more detailed, two-dimensional (2D) free energy surface constructed from histograms of the charge−charge separation distance defined above, and the hydrophobic−hydrophobic separation distance, defined as the distance between the two methyl groups of the two molecules.[73] Each histogram ranged from 2.1 to 28 Å, with bins of 0.1 Å width. As in our previous work, the solute−solute configurational entropy term,[73] which always strongly favors the dissociated state, was removed from consideration by comparing the MD-derived 2D histogram with a reference 2D histogram constructed by 100 million random placements of the two molecules into the same simulation box. The MD-derived histogram (which describes the solute−solute distribution obtained when the two solutes interact with each other in water) and the reference histogram (which describes the distribution expected when the two solutes are noninteracting in a vacuum) are used together to calculate the (excess) free energy of interaction for the ith 1D FES bin according to the equation: $\Delta G^\circ(i,j) = -\mathrm{RT}\ \ln[P_{\mathrm{interacting}}(i)/P_{\mathrm{noninteracting}}(i)]$ or the i,jth 2D FES bin according to the equation $\Delta G^\circ(i,j) = -\mathrm{RT}\ \ln[P_{\mathrm{interacting}}(i,j)/P_{\mathrm{noninteracting}}(i,j)]$, where P indicates the probability of finding the two solutes at the separation distance(s) covered by the histogram bin. The resulting relative 2D-FESs were placed on an absolute scale using a protocol similar to the one we previously described:[73] free energy offsets were obtained from a linear regression between the MD-derived and continuum electrostatic-derived direct interaction free energies performed using histogram bins in which both the intercharge and intermethyl distance were between 10 and 15 Å (full details of the continuum solvent calculations are provided below).

As shown in our previous work, one complication of the use of PME electrostatics in MD simulations is that long-range electrostatic interactions between the solutes occur not only "directly" (i.e., between the two copies that are closest to each other) but also "indirectly" (i.e., with periodic images), and if no account is taken of these long-range indirect interactions, an incorrect view of the long-range direct interaction can be obtained.[73] In our previous work, we corrected for the presence of the periodic, indirect interactions by use of Poisson calculations in which two additional "layers" of solute images were included. In the present work, we have used a simpler but better protocol that makes use of the continuum electrostatics program DelPhi:[81,82] this program has the ability to rapidly perform Poisson calculations both with and without periodic boundary conditions. In fact, DelPhi's speed was found to be sufficient enough that it could be used to perform calculations on all 5 million structural snapshots from each MD simulation. The indirect energy for each snapshot was therefore obtained by taking the difference of the electrostatic energy computed from two near-identical Delphi calculations: one of the system with periodic boundary conditions applied in all three dimensions and one without periodic boundary conditions; importantly, all other parameters, including the grid mapping of the molecules, were identical in both calculations. The total number of solutions of the Poisson equation obtained during this analysis therefore amounted to 220 million. In all calculations, the grid spacing was set to 1 Å, and the molecule dielectric constant was set to 2; the solvent dielectric constant was set to the appropriate value for water at the temperature of interest (see below).[83] It is to be noted that the comparatively coarse grid spacing of 1 Å is acceptable for the calculations described above owing to the fact that their purpose is to calculate comparatively long-range electrostatic interactions between periodic images: although the use of a coarse grid would certainly lead to errors in calculations of the *direct* interaction between the two molecules, these errors would exactly cancel when calculations performed in nonperiodic and periodic conditions are compared. Having calculated indirect energy contributions for all 5 million snapshots obtained at each temperature,

2D-FESs describing these contributions could be constructed and subtracted from the 2D-FESs computed directly from the MD simulation data: the final, resulting 2D-FESs shown in the Results therefore describe only the thermodynamics of direct interaction between a single pair of interacting molecules.

Thermodynamic Characterization. To obtain the additional thermodynamic parameters ΔH, ΔS, and ΔC_p, the ΔG values obtained at the different temperatures were fit to the Gibbs−Helmholtz equation:[50,52]

$$\Delta G(T) = \Delta H_0 + \Delta C_P(T - T_0) - T\Delta S_0 - T\Delta C_P \ln(T/T_0)$$

where T_0 is a reference temperature (chosen in this case to be 50 °C since it is at the center of the temperature range studied) and ΔH_0 and ΔS_0 are the respective interaction enthalpies and entropies at that temperature. Nonlinear fits of the simulation data to the above equation were conducted independently for all histogram bins by minimizing the mean square deviation between the ΔG values obtained from the MD simulations and the ΔG values predicted by the Gibbs−Helmholtz equation, allowing ΔC_p, ΔH_0, and ΔS_0 to be free parameters. In the case of the acetate−methylammonium system, since these fits were performed independently for each bin in the 2D-FES, it was possible in turn to construct two-dimensional surfaces for ΔC_p, ΔH_0, and ΔS_0 (see the Results). All fits were conducted with Microsoft Excel (http://office.microsoft.com). As written above, and as used in previous simulation studies,[50,52,55] ΔC_p is assumed to be independent of temperature. In the present study, however, we found that the precision of the simulation data, when plotted as a function of a single distance, was sufficiently high that it was also possible to discern a meaningful temperature dependence to ΔC_p by assuming a simple linear dependence on temperature, i.e., $\Delta C_p(T) = \Delta C_{p,0} + \alpha T$ (see the Results).

Continuum Solvation Calculations. To test whether the acetate−methylammonium 2D-FESs obtained from costly, explicit-solvent MD simulations could be reproduced by a faster implicit-solvent modeling scheme, additional calculations were performed with a combined continuum electrostatic + surface-area-based hydration model that one of us previously used[84,85] at the temperatures −12.5°, 25°, 62.5°, and 100 °C. "Direct" electrostatic contributions to association were computed using the Poisson−Boltzmann electrostatics program UHBD[86] following a protocol very similar to that used in our previous work.[73] Briefly, 15 structural snapshots from each bin on the 25 °C 2D-FES (obtained with the TIP3P water model) were randomly selected, and each was used to perform a series of Poisson calculations of (a) the methylammonium alone, (b) the acetate alone, and (c) the two molecules together, in the aqueous phase at each temperature of interest. All Poisson calculations were conducted in two stages: first, a 50 × 50 × 50 grid of spacing 1 Å was used, with boundary potentials assigned using the Coulombic approximation, and then a second, "focusing" calculation using a 100 × 100 × 100 grid of spacing 0.25 Å was performed. In all cases, the dielectric constants of the solutes were set to 2, while that of the solvent was set to the appropriate value for water at the temperature of interest, e.g., 78.45 for 25° and 55.57 for 100 °C.[83] The atomic charges used in all calculations were the same as those used in the MD simulations, and the atom radii were obtained from a previous extension to the PARSE parameter set[87] made by one of us to allow the parameter set's use at a wide range of temperatures.[84] In the extended PARSE model, the atomic radii are temperature dependent, increasing in size through the use of a radius scaling factor (RSF) as the temperature increases: different RSFs are applied to the atoms of the amino, carboxyl and methyl groups. As in the original PARSE scheme,[87] an additional surface-area based term was used to model nonelectrostatic contributions to association. In order to calculate these contributions at each temperature of interest, UHBD was first used to compute changes in solvent accessible surface areas due to association (with a probe radius of 1.4 Å), and these were then scaled by appropriate proportionality constants, $\gamma_{aliphatic}$ and γ_{polar}, parametrized in our previous work.[84] The total implicit-solvent interaction free energy at each bin of the 2D-FES was then obtained as the sum of these electrostatic and nonelectrostatic contributions: $\Delta G = \Delta G_{elec} + \Delta G_{nonelec}$.

Results

Temperature Dependence of the Free Energies of Association. Unconstrained molecular dynamics (MD) simulations of acetate−methylammonium and methane−methane pairs in explicit solvent were performed at 11 temperatures with two different but commonly used water models. The resulting computed excess free energies of interaction, ΔG, plotted versus the intermolecular distance, are shown for both types of association and for both types of water model in Figure 1 (note that different scales have been used for the two interaction types). As noted previously from simulations performed at 25 °C,[63] the computed ΔG for forming the salt bridge contact (left-hand panels) is significantly more favorable than for forming the methane−methane contact (right-hand panels); this remains true for all temperatures and with both water models. For both types of interaction, there is a general tendency for the ΔG's to become progressively more favorable as the temperature increases. This trend, while operative at all intermolecular distances, is especially apparent for the direct contact free energy minima, which are located at separation distances of 3.3 Å and 3.8 Å for the salt bridge and methane−methane interactions, respectively; the temperature dependencies of these contact minima are highlighted as insets in Figure 1. The latter plots also lead to two more significant observations. First, and most obviously, the plots of ΔG versus T are nonlinear and curve in opposite directions for the hydrophobic and charge−charge interactions. Second, the extents of curvature are much greater for the simulations performed with the TIP5P water model than for the TIP3P model. As is considered in more detail later, these aspects of the plots report directly on the different ΔC_p's of interaction.

Performing global fits of the free energy data to the Gibbs−Helmholtz equation provides smoothed estimates of the ΔG of interaction at all temperatures (see the Methods section); the quality of such fits, for both the charge−charge and hydrophobic interactions, can be assessed by examining

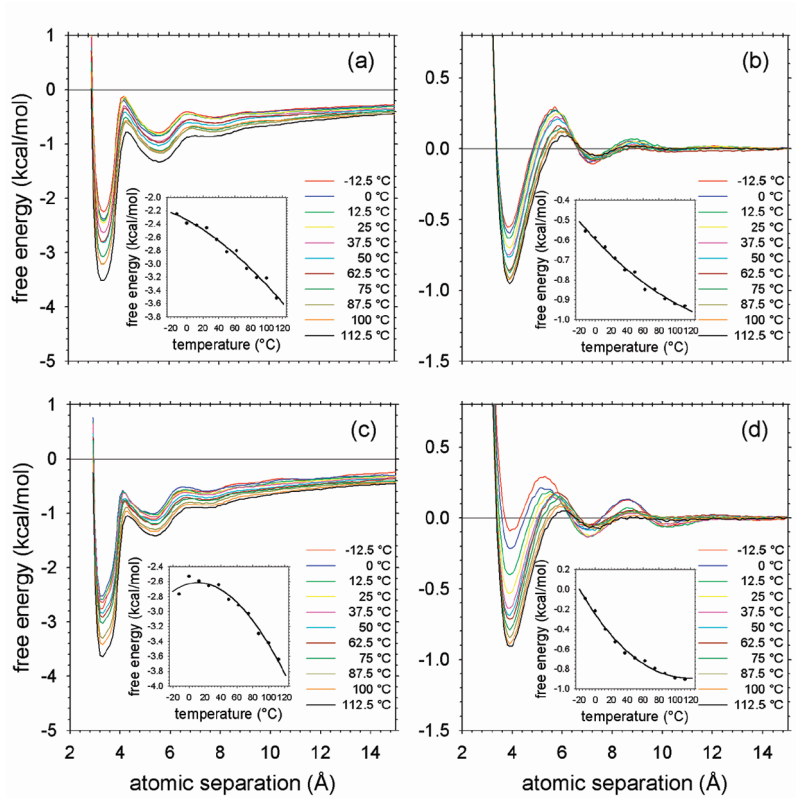

Figure 1. Excess free energy of interaction of acetate−methylammonium (a, c) and methane−methane pairs (b, d) plotted as a function of the intermolecular distance for all temperatures in the range −12.5° to 112.5 °C. Panels a and b are for the TIP3P water model; panels c and d are for TIP5P. The insets show a close-up of the behavior of the global free energy (contact configuration) minima.

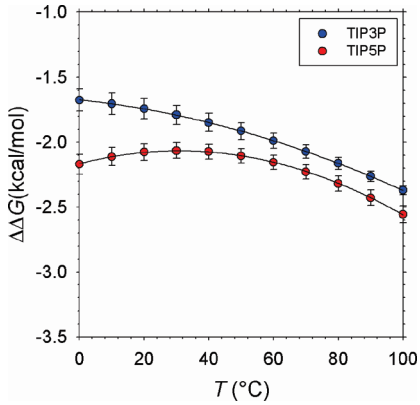

Figure 2. Plot of the difference between the smoothed ΔG values for the direct charge−charge and hydrophobic contacts plotted versus temperature for TIP3P (blue circles) and TIP5P (red circles) water models. Error bars represent the standard deviation obtained from three independent Gibbs−Helmholtz fits: for the charge−charge contact, fits were performed using data at separation distances of 3.2, 3.3, and 3.4 Å; for the hydrophobic contact, fits were performed using data at separation distances at 3.7, 3.8, and 3.9 Å.

the solid lines of the insets to Figure 1. In Figure 2, we show the difference, $\Delta\Delta G$, between the smoothed ΔG values of the direct charge−charge and hydrophobic interactions as a function of the temperature for the two water models. The $\Delta\Delta G$ is negative at all temperatures due to the considerably greater affinity computed for the charge−charge interaction (see above). But a much more interesting result concerns the temperature dependence of this $\Delta\Delta G$. Between ∼40° and 100 °C, both the TIP3P and TIP5P water models predict essentially identical behavior: the $\Delta\Delta G$ increases in magnitude as the temperature increases, indicating that, relative to the hydrophobic contact, the charge−charge contact becomes progressively stronger at higher temperatures.[63] Between 40° and 0 °C, however, there is a clear difference between the two water models: while the TIP3P curve continues to show a significant temperature dependence, the TIP5P curve flattens completely and predicts effectively no change in the *relative* strengths of charge−charge and hydrophobic interactions over this temperature range. As is considered in detail in the Discussion section, this result may have implications for understanding the relative roles played by hydrophobic and salt bridge interactions in proteins from psychrophilic, mesophilic, and hyperthermophilic organisms.

Gibbs−Helmholtz Fits of the 1D Free Energy Functions. Globally fitting ΔG data to the Gibbs−Helmholtz equation not only allows smoothed estimates of ΔG to be obtained but it also allows a deeper thermodynamic understanding to be obtained from examination of the fitted ΔH, ΔS, and ΔC_p values (see the Methods section). The resulting computed ΔH's of the charge−charge and hydrophobic interactions are plotted versus temperature in Figure 3a; corresponding plots of the ΔS are shown in Figure 3b. The different *qualitative* temperature dependences of the charge−charge and hydrophobic interactions are apparent from both figures: the slope of the ΔH for the charge−charge interaction

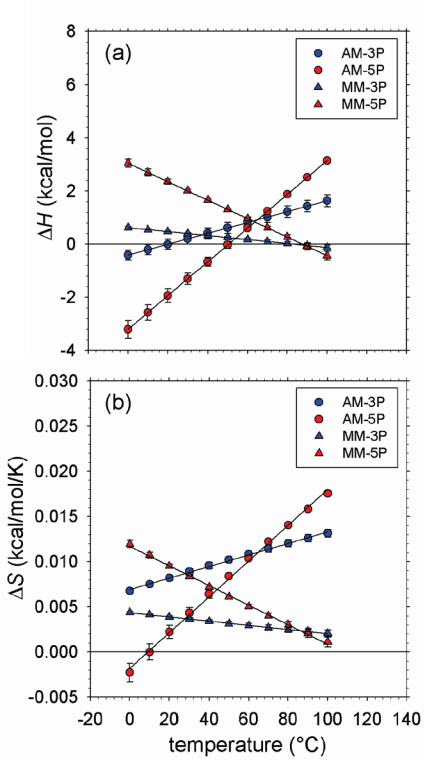

Figure 3. Plots of ΔH (a) and ΔS (b) versus temperature for acetate−methylammonium (AM; circles) and methane−methane (MM; triangles) systems. Results for TIP3P (3P) and TIP5P (5P) water models are shown as blue and red symbols, respectively. Error bars were computed in the same way as described in the legend to Figure 2.

(circles), for example, is of opposite sign to the slope of the ΔH for the hydrophobic interaction (triangles). The significant *quantitative* differences between the results obtained with the two water models, on the other hand, can be seen by comparing the very different slopes of the red (TIP5P) and blue (TIP3P) symbols.

One issue that is especially notable in Figure 3a and b concerns the temperature at which the ΔH and ΔS of the *hydrophobic* interaction approach zero (triangles). Experimentally, it has been shown that the values of the hydration ΔH, of unfolding of a wide range of proteins tend to zero at ∼90 °C, and that the corresponding ΔS values tend toward zero at 112−118 °C;[33,35,36,88−90] the origins of this effect, and what it tells us about the hydrophobic effect, have been the subject of considerable study.[33,35,36,91−95] Interestingly, the ΔH and ΔS values of the hydrophobic interaction computed with the TIP5P water model reach zero, or are extrapolated to reach zero, at ∼87 °C and ∼108 °C, respectively, both of which values are in very good agreement with the experiment. The ΔH and ΔS values obtained with the TIP3P water model, on the other hand, reach zero at ∼83 °C and ∼187 °C, which is qualitatively correct (in the sense that the zero-point temperature for ΔS is higher than that for ΔH), but in poor quantitative agreement. On the basis of this comparison, therefore, one might conclude that the TIP5P water model gives a more realistic description of the effects of temperature on biomolecular association thermodynamics.

As noted above, the curvatures apparent in the insets of Figure 1 are indicative of a nonzero ΔC_p for the charge−charge and hydrophobic interactions. For the TIP5P water model, the ΔC_p values obtained from Gibbs−Helmholtz fits—in which ΔC_p is assumed to be temperature-independent—are +60 and −35 cal/mol/K for the charge−charge and hydrophobic contact interactions, respectively; for TIP3P, the corresponding numbers are +19 and −6 cal/mol/K, respectively. Both water models therefore correctly reproduce the fact that the ΔC_p for charge−charge and hydrophobic interactions, being dominated by hydration terms, will be of opposite sign,[24,26,30,96−98] with the TIP5P model, as expected, producing the larger estimates. For the hydrophobic interaction, the computed ΔC_p values can be compared with values derived by regression analyses of experimental protein folding thermodynamics data[8,22−24] and small-molecule solubility data.[99] The experimental data are typically expressed in a form normalized by the degree of buried nonpolar surface area; typical regressed values of the nonpolar ΔC_p contributions are −1.9,[8] −1.4,[22] −1.2,[23] and −2.1[24] J/mol/K/Å^2. Normalizing our computed estimates by the amount of surface area buried in the direct contact configuration (64.3 Å^2), we obtain ΔC_p contributions of −2.3 and −0.4 J/K/mol/Å^2 for TIP5P and TIP3P, respectively; as might have been anticipated, therefore, the two water models give estimates that straddle the corresponding experimental estimates.

Analysis of the computed ΔC_p behavior can in fact be taken a stage further by exploring potential temperature dependences of the charge−charge and hydrophobic ΔC_p values (see the Methods section); this has been done by repeating the Gibbs−Helmholtz fits under the assumption that ΔC_p is a *linear* function of temperature. For the TIP3P water model, the much smaller absolute values of the ΔC_p's make it difficult to be certain of any trend, but for TIP5P a clear temperature dependence is apparent: for all interaction distances less than 8 Å, the ΔC_p of the charge−charge interaction becomes progressively more positive as temperature increases while ΔC_p of the hydrophobic interaction becomes progressively more negative (Figure 4a). The temperature dependence of ΔC_p for both types of interaction at their contact distances are illustrated in Figure 4b and compared with Privalov and Makhatadze's experimental estimates[34] of the polar and nonpolar ΔC_p contributions made to protein folding in Figure 4c. The behavior obtained with the TIP5P water model is in surprisingly good qualitative agreement with that seen experimentally.

A More Detailed View of the Acetate−Methylammonium Interaction. A more detailed view of the effects of temperature on the interaction thermodynamics of the acetate−methylammonium pair offers an opportunity to examine the *simultaneous* operation of charge−charge and hydrophobic interactions.[73] This can be done by constructing two-dimensional free energy surfaces (2D-FESs) in which the x coordinate is the charge−charge distance (the $C_{carboxyl}-N_{amino}$ distance) and the y coordinate is the distance between the hydrophobic groups (the $C_{methyl}-C_{methyl}$ distance). Representative two-dimensional free energy surfaces (2D-FESs) obtained with the TIP5P water model are shown

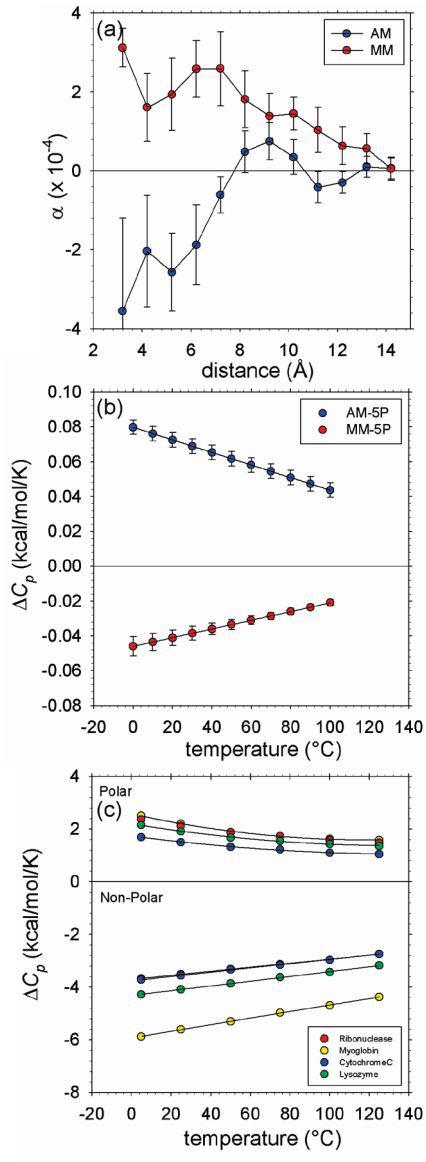

Figure 4. (a) Temperature dependence of ΔC_p, α, plotted versus intermolecular distance for acetate−methylammonium (AM; blue circles) and methane−methane (MM; red circles) systems, data obtained with the TIP5P water model. (b) Computed ΔC_p for the direct charge−charge (AM; blue circles) and hydrophobic (MM; red circles) contacts versus temperature, data obtained with the TIP5P water model. (c) Experimental ΔC_p versus temperature for cytochromeC (blue circles), ribonuclease (red circles), lysozyme (green circles), and myoglobin (yellow circles) folding, data taken from ref 34. Error bars shown in a represent the standard error obtained from the Gibbs−Helmholtz fit performed in SigmaPlot.[122] Error bars for b were computed in the same way as described in the legend to Figure 2.

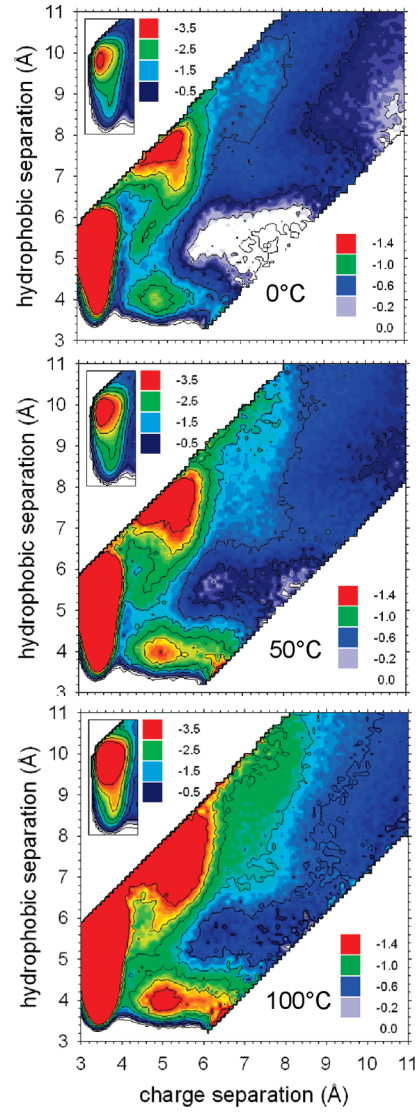

Figure 5. 2-Dimensional (excess) interaction free energy surfaces (2D-FESs) for acetate−methylammonium for three temperatures, data obtained with the TIP5P water model. The insets show close-ups of the 2D-FES in the region of the charge−charge contact, replotted on energy scales that allow identification of the global minimum.

for 0°, 50°, and 100 °C in Figure 5; complete results for all 11 temperatures and for both water models are provided in Figures S2 and S3 (Supporting Information). On each 2D-FES, there are three pronounced minima. The first, the global minimum configuration, is the direct charge−charge contact (i.e., a conventional salt bridge) located at coordinates (x, 3 Å; y, 5 Å) on the 2D-FES; the two other (local) minima are a solvent-separated charge−charge interaction at coordinates (x, 5.5 Å; y, 7 Å) and a broad methyl−methyl hydrophobic contact at (x, 5−6 Å; y, 4 Å). The same features appear on the 2D-FESs obtained with the TIP3P water model, with the only notable differences—such as a broader minimum for the methyl−methyl contact—being caused by TIP5P having a lower free energy barrier to the dissociation of the charge−charge contact (apparent from comparing Figure 1a and c; see also Figure S4, Supporting Information).

As anticipated from the behavior of the one-dimensional free energy functions shown in Figure 1, increasing the temperature stabilizes all three of the local minima on the 2D-FES. The differing degrees of stabilization of the three local minima, however, become more apparent in the form of 2D-FES-difference maps obtained by subtracting 2D-FESs at 100 and 25 °C (Figure 6a,b). From such plots, it is apparent that for *both* water models the direct charge−charge interaction is much more strongly stabilized by increasing temperature than the other modes of interaction. Interestingly, a plot of the data points from the TIP3P 2D-FES-difference

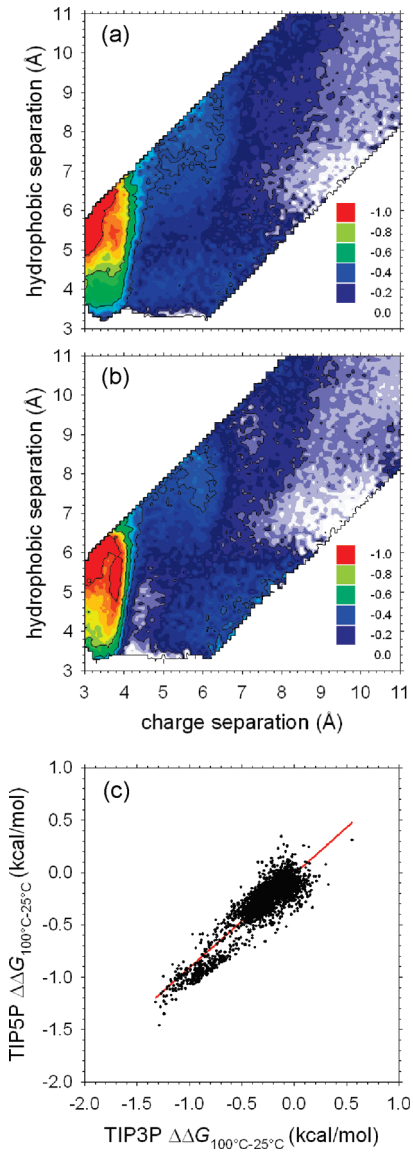

Figure 6. (a) 2D-FES difference surface ($\Delta\Delta G_{100-25°C}$) for the TIP3P water model. (b) 2D-FES difference surface ($\Delta\Delta G_{100-25°C}$) for TIP5P. (c) Correlation of data points from the TIP5P 2D-FES difference surface with those from the corresponding TIP3P 2D-FES difference surface; only data points with a charge−charge separation between 2.9 and 20 Å are plotted. The red line is the linear regression line with slope = 0.8934, intercept = −0.0182, and R^2 = 0.8306.

map versus the corresponding data points from the TIP5P 2D-FES-difference map shows—for the temperature range 25° to 100 °C—a high degree of correlation (R^2 = 0.83), with a slope (0.89) indicating a slightly greater temperature dependence for the TIP3P model (Figure 6c). As explored in detail below, these 2D-FES-difference maps provide a critical test for continuum solvation models intended to describe the temperature dependence of biomolecular interactions at high temperatures.

As with the 1D free energy functions, it is possible to extract further thermodynamic information by globally fitting the 2D-FESs to the Gibbs−Helmholtz equation: doing so allows 2D surfaces for the ΔH, ΔS, and, most importantly, the ΔC_p of the interaction to be derived (see the Methods section). Examples of the kinds of fits that are obtained are shown in Figure S5 (Supporting Information) for the three major free energy minima on the TIP5P 2D-FES; similar results obtained with the TIP3P model are shown in Figure S6 (Supporting Information). As might be expected, the best fits to the Gibbs−Helmholtz equation are obtained in those regions on the 2D-FESs that are most frequently sampled during the MD simulations: for example, in the case of the three regions shown in Figures S5 and S6 (Supporting Information), the fit is clearly better for the global minimum configuration. This connection between sampling efficiency and quality of the Gibbs−Helmholtz fits is shown in a 2D surface representation for both water models in Figure S7 (Supporting Information): from these plots, the tendency for errors to be greatest in the regions of the surface that are poorly sampled is clear, especially in those regions corresponding to desolvation barriers. In fact, for certain parts of the 2D-FES, the adequacy of sampling was questionable for the TIP5P water model at the three lowest temperatures studied (−12.5°, 0°, and 12.5 °C); these 2D-FESs were therefore omitted from the global Gibbs−Helmholtz fits. Despite this caution—which, it should be noted, does *not* apply to the free energies when plotted as a function of a *single* dimension (Figure 1)—the ΔG values computed directly from these low temperature simulations were usually in good agreement with the ΔG values extrapolated from the Gibbs−Helmholtz fits to the 8 higher temperatures (see open symbols in Figure S5).

Two-dimensional surfaces illustrating the ΔH and $T\Delta S$ of interaction at a number of temperatures are shown in Figures S8 and S9 (Supporting Information); the more interesting quantity to examine however is the heat capacity, ΔC_p, which is shown in a 2D representation for both water models in Figure 7. The TIP3P water model (Figure 7a) produces a very slightly positive ΔC_p of interaction over much of the 2D surface. The TIP5P water model (Figure 7b), in contrast, produces a strongly positive ΔC_p for the direct charge−charge contact, and a strongly negative ΔC_p for the hydrophobic contact (which matches well with the behavior seen in the methane−methane simulations). With the TIP5P model, therefore, it is possible to discern distinct modes of interaction between the same two molecules that have qualitatively different ΔC_p behaviors; moreover, effecting such a qualitative change in the ΔC_p requires only a shift in relative orientation of the two molecules of a few Ångstroms.

Comparison with Implicit Solvation Calculations. The availability of explicit solvent free energy surfaces computed over a range of temperatures provides an excellent opportunity to test the ability of implicit (continuum) solvent models to capture temperature dependent effects. In what follows, therefore, the interaction thermodynamics obtained from MD are compared with corresponding results obtained using the current "gold standard" implicit solvent model, the Poisson(−Boltzmann) method.[100−102] Two sets of Poisson calculations were carried out: one in which the only temperature-dependent parameter in the calculations was the solvent dielectric constant and one in which, additionally, the atomic radii were adjusted by a temperature-dependent radius scaling factor (RSF) empirically derived previously[84] to reproduce the experimental hydration free energies of

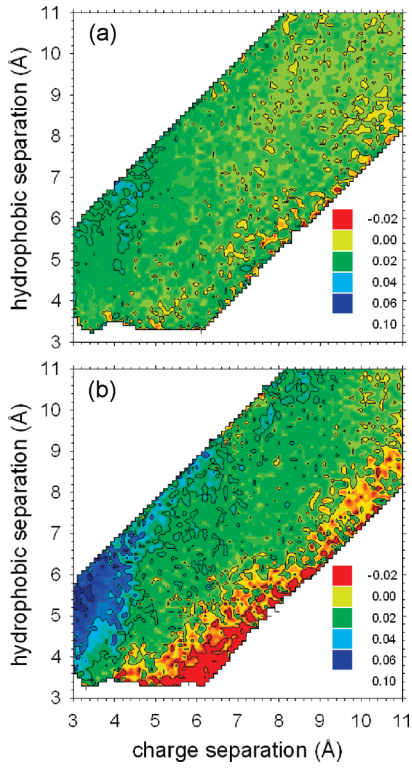

Figure 7. 2D surfaces showing the heat capacity change of interaction, ΔC_p, for the (a) TIP3P and (b) TIP5P water models.

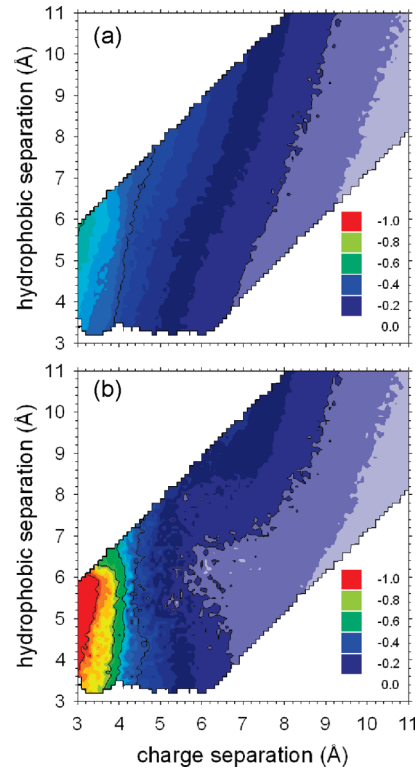

Figure 8. 2D-FES difference surfaces ($\Delta\Delta G_{100-25°C}$) obtained from Poisson−Boltzmann calculations performed (a) without radius scaling factor (RSF) and (b) with RSF.

amino acids over a wide range of temperatures. Nonpolar contributions to the acetate−methylammonium interaction were calculated using a temperature-dependent solvent accessible surface area (SASA) term (see the Methods section).

2D-FES-difference maps showing the effects of changing the temperature from 25° to 100 °C are shown for both Poisson calculation protocols in Figure 8a and b; these implicit-solvent surfaces should be compared with the explicit-solvent surfaces shown in Figure 6a and b. Such a comparison indicates that treating the atomic radii as temperature dependent with the RSF results in much better agreement with the explicit solvent MD results, especially in terms of describing the temperature dependence of the direct charge−charge interaction. In fact, linear regression of the Poisson-computed free energy differences with those obtained from the TIP5P simulations shows significant improvements in the slope, the intercept, and the r^2 value when the RSF is included (see Figure 9a and b, respectively). A qualitatively identical finding is obtained when the implicit solvent results are compared instead to the TIP3P results (Figure S10, Supporting Information).

Discussion

As noted in the Introduction, the studies reported here have been conducted with two water models that have been chosen to provide what are thought to be extreme descriptions of the likely effects of temperature on biomolecular interactions.[55] While significant differences are certainly found between the two models (see below), it is striking that they make very similar predictions of the temperature's effects on

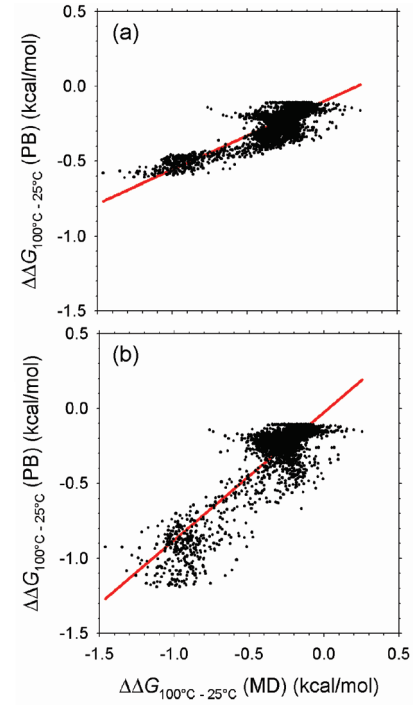

Figure 9. Correlation of $\Delta\Delta G_{100-25°C}$ calculated from Poisson−Boltzmann calculations and from TIP5P MD simulations. (a) PB calculations performed without RSF: slope = 0.4513, intercept = −0.1059, $r^2 = 0.7313$. (b) PB calculations performed with RSF: slope = 0.8506, intercept = −0.0263, $r^2 = 0.7873$.

the free energies of the hydrophobic and charge−charge interactions at medium-to-high temperatures. Increasing the

temperature from 25° to 100 °C changes the ΔG of the direct charge−charge interaction by −0.76 and −0.77 kcal/mol with the TIP3P and TIP5P models, respectively (Figure 1a,c) and changes the ΔG of the methane−methane interaction by −0.23 and −0.36 kcal/mol with TIP3P and TIP5P, respectively (Figure 1b,d). Importantly, as we discuss next, this close correspondence between the two explicit solvent water models at medium-to-high temperatures allows unambiguous conclusions to be drawn about the use of implicit solvent (Poisson) calculations for investigating the effects of high temperatures on biomolecular interaction thermodynamics.

Poisson and Poisson−Boltzmann calculations are widely used to provide insights into electrostatic contributions to biomolecular interactions[100−102] and have been especially exploited to investigate the contributions of salt bridges to the stability of proteins from hyperthermophilic organisms.[85,103−108] A number of the latter studies have attempted to compare salt bridge interaction thermodynamics at low and high temperatures by comparing calculation results[105,107,108] obtained with the solvent dielectric constant set to the appropriate experimental value for water (the dielectric constant of water changes from 87.9 at 0 °C to 55.6 at 100 °C[83]). Ideally, altering the solvent dielectric constant in this way would be the *only* change required in order for implicit solvent models to capture accurately the effects of changing temperature on interaction thermodynamics. Previous work carried out by one of us,[84] however, found that the temperature dependence of amino acid *hydration* free energies was systematically underestimated (compared with the experiment) when this approach was followed; in order to obtain agreement with the experiment, it was found necessary to adjust the atomic radii by an empirically determined radius scaling factor[84] (RSF). Since changes in hydration play such a critical role in determining the thermodynamics of interactions between charged residues,[85,103] it is to be anticipated that the requirement for adjustable atomic radii might reappear in attempts to match temperature dependent changes in *association* free energies. The explicit solvent MD results reported here have provided the opportunity to examine this issue. While the overall agreement between the 2D-FES-difference maps obtained from explicit solvent (Figure 6) and implicit solvent (Figure 8) calculations is far from perfect, the overall trend is pretty clear: the free energy change obtained when the solvent dielectric constant is the *only* parameter changed in the implicit solvent calculations is much smaller than that obtained from explicit solvent simulations, but the free energy change obtained when the RSF is used is much closer in magnitude. With regard to continuum solvation calculations, therefore, the basic conclusion to be drawn from the present study is the following. On the basis of two independent lines of evidence—comparisons with (a) the experimental temperature dependence of amino acid hydration free energies[84] and (b) the MD-simulated temperature dependence of salt bridge association free energies (shown here)—a strong case can be made that atomic radii should be adjusted with a RSF in Poisson or Poisson−Boltzmann calculations aimed at modeling temperature dependent changes in biomolecular thermodynamics.

As noted above, this conclusion can be drawn with confidence owing to the fact that the quite different TIP3P and TIP5P water models make essentially identical predictions about the overall magnitude of ΔG changes in the range 25° to 100 °C; another way of saying this is that the computed first derivative of ΔG with respect to temperature (in this temperature range) is very similar for both models. Where the two water models produce quite different results is in the more subtle quantity ΔC_p, which describes the second derivative of ΔG with respect to temperature (i.e., its curvature). The next question to ask is of course which of the ΔC_p predictions, if any, should be believed? Owing to the fact that the TIP5P water model was specifically devised in order to correct inadequacies in the treatment of temperature effects on water's density,[70] one might immediately anticipate that it would also provide the more accurate description of temperature effects on interaction thermodynamics. Certainly, we know from the work of others that TIP5P provides a good description of the temperature dependence of water's dielectric constant. Specifically, it has been shown to produce dielectric constant values of 82 and 60 at 25 and 100 °C, respectively,[70] which compare well with the experimental values of 78.5 and 55.6;[83] unfortunately, we cannot make a corresponding comparison for TIP3P as we have been unable to find estimates of its dielectric constant at 100 °C. An additional piece of quantitative evidence in favor of TIP5P is reported here: we find that the temperatures at which ΔH and ΔS of the hydrophobic interaction equal zero are in good accord with experimental estimates for the TIP5P model but are not for TIP3P. Other observations provide suggestions, but not outright proof, that TIP5P's description is better than that of TIP3P. With the acetate−methylammonium system, for example, only the TIP5P model provides clear evidence of differently signed ΔC_p's for the charge−charge and methyl−methyl interactions. With both systems, only the TIP5P model gives a discernible trend in the temperature dependence of the ΔC_p's of interaction, and this, in turn, is in good qualitative correspondence with the trend seen in the experimental data.[34]

That said, there are other aspects of behavior of the two water models that lead to more equivocal conclusions. For example, a recent comprehensive simulation study of the heat capacity change, ΔC_p, accompanying the *hydration* of methane (modeled with the OPLS united atom model) produced estimates of 145 and 265 J/K/mol for the TIP3P and TIP5P water models, respectively.[55] The experimental estimates of the same quantity range from 209 to 242 J/K/mol[99] and so lie somewhere in between the predictions of the two models. Similarly, as outlined in the Results section, comparison of the computed ΔC_p values of the hydrophobic interaction obtained with the two water models (−2.3 and −0.4 J/K/mol/Å^2 for TIP5P and TIP3P, respectively) shows that they lie on either side of estimates obtained from regressions of experimental data.[8,22−24] There are even some respects in which TIP5P is clearly not as good as TIP3P. For example, the freezing and boiling points reported recently for the TIP3P water model (269 and 357 K, respectively[109]) are considerably better than those reported in the same work

for the TIP5P model (266 and 337 K, respectively;[109] the latter has also been independently estimated at 348 K[110]). In addition, the computed heat capacity of *pure* TIP5P water (29.2 J/K/mol) is in somewhat worse agreement with the experiment (18.0 J/K/mol) than are the heat capacities of the simpler TIP3P, SPC, and TIP4P water models (C_p values of 20.0, 20.2, and 20.4 J/K/mol, respectively).[111] This latter result indicates, as noted by Mahoney and Jorgensen, that a better treatment of structural properties does not always lead to a better modeling of thermodynamic quantities.[70] It is certainly possible, therefore, that other water models might reproduce aspects of temperature-dependent thermodynamics somewhat better than TIP5P.

Before leaving the subject of ΔC_p, it is worth noting that the same regression studies of experimental data referred to above have also indicated that, when expressed in units of buried surface area, the magnitude of the (positive) contribution to ΔC_p made by the burial of polar groups is considerably *smaller* than that of the (negative) contribution to ΔC_p made by the burial of nonpolar groups: the reported respective ΔC_p values for burial of polar vs nonpolar groups are +1.1 vs −1.9 J/mol/K/Å,[2,8] +0.7 vs −1.4 J/mol/K/Å,[2,22] +0.4 vs −1.2 J/mol/K/Å,[2,23] and +0.9 vs −2.1 J/mol/K/Å.[2,24] It is noticeable that the magnitude of the MD-computed ΔC_p for the charge−charge interaction is some 2−3 times *larger* than that of the hydrophobic interaction: with the TIP5P model, the ΔC_p for formation of the direct charge−charge contact is +60 cal/mol/K while that for formation of the hydrophobic (methane−methane) contact is −35 cal/mol/K. For TIP3P, the ΔC_p for formation of the direct charge−charge contact is +19 cal/mol/K, while that for formation of the hydrophobic (methane−methane) contact is −6 cal/mol/K. The most likely explanation of this apparent discrepancy is simply that, in the regressions of the experimental data, the "polar" contribution encompasses neutral, hydrogen bonding groups (especially the peptide backbone) in addition to charged groups; formation of neutral hydrogen bonding interactions, which have not been studied here, are likely to make much smaller contributions to heat capacity changes.

The qualitative difference between the ΔC_p values associated with the formation of charge−charge and hydrophobic contacts has consequences for their relative stabilities at both high and low temperatures (Figure 2). The finding that a salt-bridge interaction becomes progressively more stable than a hydrophobic interaction at high temperatures (∼40−100 °C) is not especially new, since we have found much the same result previously using both implicit[85] and TIP3P-based explicit solvent simulations.[63] It is nevertheless notable, however, that the same basic result is obtained with the TIP5P water model, despite the large quantitative differences between the TIP5P and TIP3P ΔC_p values. This indicates that the basic conclusions drawn previously[63] are not dependent on the water model. The thermodynamic behavior obtained in both the present and previous simulations provides an attractive explanation—though not the only one imaginable[104−107]—for the unusual abundance of salt bridge interactions in proteins from hyperthermophilic organisms.[4,112]

The more novel result of the present study is that, with the TIP5P water model, the relative strengths of salt-bridge and hydrophobic interactions are largely unchanged between 0° and 40 °C. Just as the preference of salt bridges for high temperatures has apparent implications for understanding the adaptation mechanisms of hyperthermophilic organisms,[4] this new finding may have implications for understanding organisms adapted to life at very low temperatures (psychrophiles). If it is indeed true that the relative stabilities of electrostatic and hydrophobic interactions remain essentially unchanged as the temperature drops to 0 °C, then there should be no selective advantage to accumulating or losing salt bridges at low temperatures: the relative numbers of salt bridges and hydrophobic interactions should therefore be very similar in mesophiles and psychrophiles. Since a number of crystal structures of proteins from psychrophilic organisms have recently become available, the accuracy of the above prediction can be directly examined. In fact, in the majority of cases that have been reported so far, the numbers of salt bridges in psychrophilic enzymes are indeed very similar to[113−115] or somewhat lower than[116−118] those found in their mesophilic homologues. One interesting exception that we know of is citrate synthase: the psychrophilic (and hyperthermophilic) versions of this enzyme have increased numbers of salt bridges relative to their mesophilic cousin, although in the case of the psychrophile, only *intra*-subunit salt bridges are found to be increased.[107] Exceptions are perhaps to be anticipated: obtaining unambiguous views of the adaptation mechanisms operating in psychrophiles is likely to be more difficult than for hypthermophiles since the former face the challenge of simultaneously retaining not only stability but also activity in their chosen environmental conditions.[1−3]

Summary

The complete thermodynamic characterization of two types of molecular interactions in the range 0° to 100 °C shows that there are areas in which typical simulation water models are likely to produce essentially identical behavior and areas in which they will differ markedly. Both water models can capture the qualitative result that the ΔC_p for formation of salt bridge interactions is positive—which is something that has not been shown before—while the ΔC_p for formation of hydrophobic interactions is negative; the models differ drastically however in their predictions of the magnitude of the ΔC_p. Both water models predict that on raising the temperature from ∼40° to 100 °C salt-bridge interactions are significantly more stabilized than are hydrophobic interactions. But they differ drastically in their predictions of what happens when the temperature drops from 40° to 0 °C. As noted above, the similarity of the models' predictions at high temperatures enables us to draw some firm conclusions regarding protocols for implicit solvent calculations at high temperatures; it also argues that for molecular dynamics simulations aimed at investigating biomolecular behavior at high temperatures the choice of water model may not be especially important. But the very significant differences observed at low temperatures on the other hand—which on balance appear to favor the TIP5P model—suggest that a closer examination of behavior at low temperatures may be important for force field development. Finally, it should be

noted that, while we have explicitly compared the thermodynamic characteristics of hydrophobic and favorable charge−charge interactions here, these are not the only types of interactions to play important roles in determining biomolecular stability. It will in particular be of interest to explore similar issues for the thermodynamics of hydrogen bonding[119] and cation−π[120,121] interactions.

Acknowledgment. The authors are grateful to Dr. Andy S. Thomas for thoughtful discussions. This work was supported by a NSF CAREER award (#0448029) to A.H.E.

Supporting Information Available: Ten supporting figures: Time course of minimum distance between molecules versus time at the two lowest temperatures; 2D-FESs at all temperatures for TIP3P and TIP5P models; difference 2D-FESs between TIP5P and TIP3P at two temperatures; Gibbs−Helmholtz fits at three minima for TIP3P and TIP5P models; 2D surface showing errors in Gibbs−Helmholtz fits; 2D surfaces showing ΔH and $T\Delta S$ at two temperatures for TIP3P and TIP5P models; correlation of PB and TIP3P free energy differences with and without RSF. This information is available free of charge via the Internet at http://pubs.acs.org/.

References

(1) Cavicchioli, R.; Siddiqui, K. S.; Andrews, D.; Sowers, K. R. *Curr. Opin. Biotechnol.* **2002**, *13*, 253–261.

(2) Feller, G.; Gerday, C. *Nat. Rev. Microbiol.* **2003**, *1*, 200–208.

(3) Siddiqui, K. S.; Cavicchioli, R. *Annu. Rev. Biochem.* **2006**, *75*, 403–433.

(4) Sterner, R.; Liebl, W. *Crit. Rev. Biochem. Mol. Biol.* **2001**, *36*, 39–106.

(5) Vieille, C.; Zeikus, G. J. *Microbiol. Mol. Biol. Rev.* **2001**, *65*, 1–43.

(6) Kumar, S.; Nussinov, R. *Cell. Mol. Life Sci.* **2001**, *58*, 1216–1233.

(7) Karshikoff, A.; Ladenstein, R. *Trends Biochem. Sci.* **2001**, *26*, 550–556.

(8) Murphy, K. P.; Freire, E. *Adv. Protein Chem.* **1992**, *43*, 313–361.

(9) Montgomery, D.; Jordan, R.; McMacken, R.; Freire, E. *J. Mol. Biol.* **1993**, *232*, 680–692.

(10) Haynie, D. T.; Freire, E. *Anal. Biochem.* **1994**, *216*, 33−41.

(11) Xie, D.; Fox, R.; Freire, E. *Protein Sci.* **1994**, *3*, 2175–2184.

(12) Viguera, A. R.; Martinez, J. C.; Filimonov, V. V.; Mateo, P. L.; Serrano, L. *Biochemistry* **1994**, *33*, 2142–2150.

(13) McCrary, B. S.; Edmondson, S. P.; Shriver, J. W. *J. Mol. Biol.* **1996**, *264*, 784–805.

(14) Loladze, V. V.; Ermolenko, D. N.; Makhatadze, G. I. *J. Mol. Biol.* **2002**, *320*, 343–357.

(15) Bhat, T. N.; Bentley, G. A.; Boulot, G.; Greene, M. I.; Tello, D.; Dallacqua, W.; Souchon, H.; Schwarz, F. P.; Mariuzza, R. A.; Poljak, R. J. *Proc. Natl. Acad. Sci. U. S. A.* **1994**, *91*, 1089–1093.

(16) Martinez, J. C.; Filimonov, V. V.; Mateo, P. L.; Schreiber, G.; Fersht, A. R. *Biochemistry* **1995**, *34*, 5224–5233.

(17) Baker, B. M.; Murphy, K. P. *J. Mol. Biol.* **1997**, *268*, 557–569.

(18) Gonzalez, M.; Bagatolli, L. A.; Echabe, I.; Arrondo, J. L. R.; Argarana, C. E.; Cantor, C. R.; Fidelio, G. D. *J. Biol. Chem.* **1997**, *272*, 11288–11294.

(19) Frisch, C.; Schreiber, G.; Johnson, C. M.; Fersht, A. R. *J. Mol. Biol.* **1997**, *267*, 696–706.

(20) Xavier, K. A.; Shick, K. A.; SmithGill, S. J.; Willson, R. C. *Biophys. J.* **1997**, *73*, 2116–2125.

(21) Jelesarov, I.; Bosshard, H. R. *J. Mol. Recognit.* **1999**, *12*, 3–18.

(22) Spolar, R. S.; Livingstone, J. R.; Record, M. T. *Biochemistry* **1992**, *31*, 3947–3955.

(23) Myers, J. K.; Pace, C. N.; Scholtz, J. M. *Protein Sci.* **1995**, *4*, 2138–2148.

(24) Makhatadze, G. I.; Privalov, P. L. *Adv. Prot. Chem.* **1995**, *47*, 307–425.

(25) Robertson, A. D.; Murphy, K. P. *Chem. Rev.* **1997**, *97*, 1251–1267.

(26) Loladze, V. V.; Ermolenko, D. N.; Makhatadze, G. I. *Protein Sci.* **2001**, *10*, 1343–1352.

(27) Nozaki, Y.; Tanford, C. *J. Biol. Chem.* **1971**, *246*, 2211–2217.

(28) Eisenberg, D.; McLachlan, A. D. *Nature* **1986**, *319*, 199–203.

(29) Ooi, T.; Oobatake, M.; Nemethy, G.; Scheraga, H. A. *Proc. Natl. Acad. Sci. U. S. A.* **1987**, *84*, 3086–3090.

(30) Makhatadze, G. I.; Privalov, P. L. *J. Mol. Biol.* **1990**, *213*, 375–384.

(31) Privalov, P. L.; Makhatadze, G. I. *J. Mol. Biol.* **1990**, *213*, 385–391.

(32) Murphy, K. P.; Privalov, P. L.; Gill, S. J. *Science* **1990**, *247*, 559–561.

(33) Murphy, K. P.; Gill, S. J. *J. Mol. Biol.* **1991**, *222*, 699–709.

(34) Privalov, P. L.; Makhatadze, G. I. *J. Mol. Biol.* **1992**, *224*, 715–723.

(35) Makhatadze, G. I.; Privalov, P. L. *J. Mol. Biol.* **1993**, *232*, 639–659.

(36) Privalov, P. L.; Makhatadze, G. I. *J. Mol. Biol.* **1993**, *232*, 660–679.

(37) Habermann, S. M.; Murphy, K. P. *Protein Sci.* **1996**, *5*, 1229–1239.

(38) Makhatadze, G. I.; Lopez, M. M.; Privalov, P. L. *Biophys. Chem.* **1997**, *64*, 93–101.

(39) Vangunsteren, W. F.; Berendsen, H. J. C. *Angew. Chem., Int. Ed. Engl.* **1990**, *29*, 992–1023.

(40) Van Gunsteren, W. F.; Bakowies, D.; Baron, R.; Chandrasekhar, I.; Christen, M.; Daura, X.; Gee, P.; Geerke, D. P.; Glattli, A.; Hunenberger, P. H.; Kastenholz, M. A.; Ostenbrink, C.; Schenk, M.; Trzesniak, D.; van der Vegt, N. F. A.; Yu, H. B. *Angew. Chem., Int. Ed.* **2006**, *45*, 4064–4092.

(41) Skipper, N. T. *Chem. Phys. Lett.* **1993**, *207*, 424–429.

(42) Skipper, N. T.; Bridgeman, C. H.; Buckingham, A. D.; Mancera, R. L. *Faraday Discuss.* **1996**, 141–150.

(43) Dang, L. X. *J. Chem. Phys.* **1994**, *100*, 9032–9034.

(44) Ludemann, S.; Schreiber, H.; Abseher, R.; Steinhauser, O. *J. Chem. Phys.* **1996**, *104*, 286–295.

(45) Ludemann, S.; Abseher, R.; Schreiber, H.; Steinhauser, O. *J. Am. Chem. Soc.* **1997**, *119*, 4206–4213.

(46) Mancera, R. L.; Buckingham, A. D. *Chem. Phys. Lett.* **1995**, *234*, 296–303.

(47) Mancera, R. L.; Buckingham, A. D.; Skipper, N. T. *J. Chem. Soc., Faraday Trans.* **1997**, *93*, 2263–2267.

(48) Rick, S. W.; Berne, B. J. *J. Phys. Chem. B* **1997**, *101*, 10488–10493.

(49) Rick, S. W. *J. Phys. Chem. B* **2000**, *104*, 6884–6888.

(50) Rick, S. W. *J. Phys. Chem. B* **2003**, *107*, 9853–9857.

(51) Shimizu, S.; Chan, H. S. *J. Chem. Phys.* **2000**, *113*, 4683–4700.

(52) Shimizu, S.; Chan, H. S. *J. Am. Chem. Soc.* **2001**, *123*, 2083–2084.

(53) Shimizu, S.; Chan, H. S. *Proteins: Struct., Funct., Genet.* **2002**, *48*, 15–30.

(54) Southall, N. T.; Dill, K. A. *Biophys. Chem.* **2002**, *101*, 295–307.

(55) Paschek, D. *J. Chem. Phys.* **2004**, *120*, 6674–6690.

(56) Paschek, D. *J. Chem. Phys.* **2004**, *120*, 10605–10617.

(57) Dill, K. A. *Biochemistry* **1990**, *29*, 7133–7155.

(58) Jorgensen, W. L.; Buckner, J. K.; Boudon, S.; Tiradorives, J. *J. Chem. Phys.* **1988**, *89*, 3742–3746.

(59) Nemethy, G.; Scheraga, H. A. *J. Phys. Chem.* **1962**, *66*, 1773–1789.

(60) Baldwin, R. L. *Proc. Natl. Acad. Sci. U. S. A.* **1986**, *83*, 8069–8072.

(61) Prabhu, N. V.; Sharp, K. A. *Annu. Rev. Phys. Chem.* **2005**, *56*, 521–548.

(62) Dang, L. X. *J. Chem. Phys.* **1992**, *97*, 1919–1921.

(63) Thomas, A. S.; Elcock, A. H. *J. Am. Chem. Soc.* **2004**, *126*, 2208–2214.

(64) Madan, B.; Sharp, K. *J. Phys. Chem.* **1996**, *100*, 7713–7721.

(65) Sharp, K. A.; Madan, B. *J. Phys. Chem. B* **1997**, *101*, 4343–4348.

(66) Sharp, K. A.; Madan, B.; Manas, E.; Vanderkooi, J. M. *J. Chem. Phys.* **2001**, *114*, 1791–1796.

(67) Gallagher, K.; Sharp, K. *Biophys. J.* **1998**, *75*, 769–776.

(68) Gallagher, K. R.; Sharp, K. A. *J. Am. Chem. Soc.* **2003**, *125*, 9853–9860.

(69) Jorgensen, W. L.; Chandrasekhar, J.; Madura, J. D.; Impey, R. W.; Klein, M. L. *J. Chem. Phys.* **1983**, *79*, 926–935.

(70) Mahoney, M. W.; Jorgensen, W. L. *J. Chem. Phys.* **2000**, *112*, b8910–8922.

(71) Berendsen, H. J. C.; Vanderspoel, D.; Vandrunen, R. *Comput. Phys. Commun.* **1995**, *91*, 43–56.

(72) Lindahl, E.; Hess, B.; van der Spoel, D. *J. Mol. Model.* **2001**, *7*, 306–317.

(73) Thomas, A. S.; Elcock, A. H. *J. Am. Chem. Soc.* **2006**, *128*, 7796–7806.

(74) Kaminski, G. A.; Friesner, R. A.; Tirado-Rives, J.; Jorgensen, W. L. *J. Phys. Chem. B* **2001**, *105*, 6474–6487.

(75) Essmann, U.; Perera, L.; Berkowitz, M. L.; Darden, T.; Lee, H.; Pedersen, L. G. *J. Chem. Phys.* **1995**, *103*, 8577–8593.

(76) Hess, B.; Bekker, H.; Berendsen, H. J. C.; Fraaije, J. *J. Comput. Chem.* **1997**, *18*, 1463–1472.

(77) Parrinello, M.; Rahman, A. *J. Appl. Phys.* **1981**, *52*, 7182–7190.

(78) Nose, S. *J. Chem. Phys.* **1984**, *81*, 511–519.

(79) Hoover, W. G. *Phys. Rev. A* **1985**, *31*, 1695–1697.

(80) Mahoney, M. W.; Jorgensen, W. L. *J. Chem. Phys.* **2001**, *114*, 363–366.

(81) Rocchia, W.; Alexov, E.; Honig, B. *J. Phys. Chem. B* **2001**, *105*, 6507–6514.

(82) Rocchia, W.; Sridharan, S.; Nicholls, A.; Alexov, E.; Chiabrera, A.; Honig, B. *J. Comput. Chem.* **2002**, *23*, 128–137.

(83) Lide, D. R. Properties of water in the range 0−100 °C. In *CRC Handbook of Chemistry and Physics*, 82nd ed.; Baysinger, G., Koetzle, T. F., Berger, L. I., Kuchitsu, K., Craig, N. C., Lin, C. C., Goldberg, R. N., Smith, A. L., Eds.; CRC Press LLC: Boca Raton, FL, 2001; pp 3−6.

(84) Elcock, A. H.; McCammon, J. A. *J. Phys. Chem. B* **1997**, *101*, 9624–9634.

(85) Elcock, A. H. *J. Mol. Biol.* **1998**, *284*, 489–502.

(86) Davis, M. E.; Madura, J. D.; Luty, B. A.; McCammon, J. A. *Comput. Phys. Commun.* **1991**, *62*, 187–197.

(87) Sitkoff, D.; Sharp, K. A.; Honig, B. *J. Phys. Chem.* **1994**, *98*, 1978–1988.

(88) Privalov, P. L.; Khechina, N. *J. Mol. Biol.* **1974**, *86*, 665–684.

(89) Privalov, P. L. *Adv. Protein Chem.* **1979**, *33*, 167–241.

(90) Privalov, P. L.; Gill, S. J. *Adv. Protein Chem.* **1988**, *39*, 191–234.

(91) Fu, L.; Freire, E. *Proc. Natl. Acad. Sci. U. S. A.* **1992**, *89*, 9335–9338.

(92) Baldwin, R. L.; Muller, N. *Proc. Natl. Acad. Sci. U. S. A.* **1992**, *89*, 7110–7113.

(93) Garde, S.; Hummer, G.; Garcia, A. E.; Paulaitis, M. E.; Pratt, L. R. *Phys. Rev. Lett.* **1996**, *77*, 4966–4968.

(94) Ashbaugh, H. S.; Truskett, T. M.; Debenedetti, P. G. *J. Chem. Phys.* **2002**, *116*, 2907–2921.

(95) Graziano, G.; Lee, B. *Biophys. Chem.* **2003**, *105*, 241–250.

(96) Cabani, S.; Gianni, P.; Mollica, V.; Lepori, L. *J. Solution Chem.* **1981**, *10*, 563–595.

(97) Bennaim, A.; Marcus, Y. *J. Chem. Phys.* **1984**, *81*, 2016–2027.

(98) Marcus, Y. *Biophys. Chem.* **1994**, *51*, 111–127.

(99) Plyasunov, A. V.; Shock, E. L. *Geochim. Cosmochim. Acta* **2000**, *64*, 439–468.

(100) Honig, B.; Nicholls, A. *Science* **1995**, *268*, 1144–1149.

(101) Cramer, C. J.; Truhlar, D. G. *Chem. Rev.* **1999**, *99*, 2161–2200.

(102) Baker, N. A. *Curr. Opin. Struct. Biol.* **2005**, *15*, 137–143.

(103) Hendsch, Z. S.; Tidor, B. *Protein Sci.* **1994**, *3*, 211–226.

(104) Xiao, L.; Honig, B. *J. Mol. Biol.* **1999**, *289*, 1435–1444.

(105) Kumar, S.; Ma, B. Y.; Tsai, C. J.; Nussinov, R. *Proteins: Struct., Funct., Genet.* **2000**, *38*, 368–383.

(106) Zhou, H. X.; Dong, F. *Biophys. J.* **2003**, *84*, 2216–2222.

(107) Kumar, S.; Nussinov, R. *ChemBioChem* **2004**, *5*, 280–290.

(108) Danciulescu, C.; Ladenstein, R.; Nilsson, L. *Biochemistry* **2007**, *46*, 8537–8549.

(109) Fennell, C. J.; Gezelter, J. D. *J. Chem. Theory Comput.* **2005**, *1*, 662.

(110) Wick, C. A.; Siepmann, J. I.; Schure, M. R. *J. Phys. Chem. B* **2003**, *107*, 10623.

(111) Jorgensen, W. L.; Jenson, C. *J. Comput. Chem.* **1998**, *19*, 1179–1186.

(112) Petsko, G. A. *Methods Enzymol.* **2001**, *334*, 469–478.

(113) Aghajari, N.; Van Petegem, F.; Villeret, V.; Chessa, J. P.; Gerday, C.; Haser, R.; Van Beeumen, J. *Proteins: Struct., Funct., Genet.* **2003**, *50*, 636–647.

(114) Arnorsdottir, J.; Kristjansson, M. M.; Ficner, R. *FEBS J.* **2005**, *272*, 832–845.

(115) Bae, E.; Phillips, G. N. *J. Biol. Chem.* **2004**, *279*, 28202–28208.

(116) Leiros, I.; Moe, E.; Lanes, O.; Smalas, A. O.; Willassen, N. P. *Acta Crystallogr., Sect. D* **2003**, *59*, 1357–1365.

(117) Violot, S.; Aghajari, N.; Czjzek, M.; Feller, G.; Sonan, G. K.; Gouet, P.; Gerday, C.; Haser, R.; Receveur-Brechot, V. *J. Mol. Biol.* **2005**, *348*, 1211–1224.

(118) Wang, E.; Koutsioulis, D.; Leiros, H. K. S.; Andersen, O. A.; Bouriotis, V.; Hough, E.; Heikinheimo, P. *J. Mol. Biol.* **2007**, *366*, 1318–1331.

(119) Myers, J. K.; Pace, C. N. *Biophys. J.* **1996**, *71*, 2033–2039.

(120) Gallivan, J. P.; Dougherty, D. A. *Proc. Natl. Acad. Sci. U. S. A.* **1999**, *96*, 9459–9464.

(121) Waters, M. L. *Biopolymers* **2004**, *76*, 435–445.

(122) *SigmaPlot*, version 10.0; Systat: Richmond, CA, 2006.

CT1000704